

Light Activation for the Versatile and Accurate Kinetic Analysis of Disassembly of Self-Immolative Spacers

Ahmed Alouane,^[a, b, c] Raphaël Labruère,^{*, [a, b, c]} Thomas Le Saux,^[c, d] Isabelle Aujard,^[c] Sylvie Dubruille,^[a, b] Frédéric Schmidt,^{*, [a, b]} and Ludovic Jullien^{*, [c, d]}

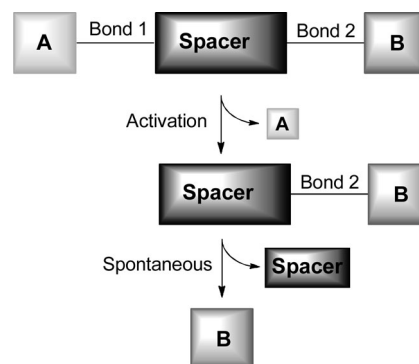
Abstract: Three procedures that rely on photoactivation are introduced to accurately analyze the disassembly kinetics of a collection of self-immolative spacer groups within the window 10^{-2} – 10^3 s. Our results are relevant for deriving quantitative structure–property relationships. In particular, we have been able to access 20 ms temporal resolution, which made possible the measurement of the shortest ever reported disassembly time for an activated self-immolative spacer.

Keywords: disassembly • fluorescence • kinetics • photochemistry • self-immolation

Introduction

Self-immolative spacers are covalent assemblies that are tailored to correlate the cleavage of two chemical bonds.^[1] Such spacer groups were first introduced to overcome chemical limitations in the design of enzymatic substrates,^[2] which typically contain two moieties that react with the enzyme (A) and report on its activity (B). When the two-part compound (A–B) cannot be obtained or cleaved by using the planned enzyme, moieties A and B can be linked together through a stable self-immolative spacer group, which decouples the enzyme-triggered bond cleavage (involving A) from the spontaneous bond cleavage that leads to the release of B (Scheme 1).

Self-immolative spacer groups have been extensively used in prodrug strategies in which B is a drug and A is a recognition motif that is responsible for the selective reaction with an enzyme.^[3] Beyond preventing steric hindrance at the enzyme cleavage site, such a design brings further degrees of freedom to tune the solubility, physiological stability, and



Scheme 1. In a self-immolative spacer, cleavage of bond 1 spontaneously causes the cleavage of bond 2. Thus, a primary event cleaves the initial precursor into three moieties: A, the spacer, and B.

metabolization of the substrate. Moreover, it also provides the ability to control the kinetics of drug release after enzymatic activation, in which the self-immolative spacer group acts as an autonomous “molecular clock”.

Self-immolative spacers are also increasingly used in the context of bioanalysis.^[4] Enzymatic activation causes the release of a probe, which shows strongly altered reporting properties. In this context, accelerating the disassembly of an activated spacer is essential. Indeed, the decomposition rate of a self-immolative spacer controls the spatial correlation between the enzyme position and the labeling location. For instance, in the emergent context of assisting surgeons by selectively labeling cells that contain specific enzymes (biomarkers),^[5] too slow a self-immolation would generate the labeling of surrounding healthy cells.

Hence, versatile and accurate kinetic analysis of the disassembly of self-immolative spacers is essential for determining their scope of application. Previous kinetic studies have already provided useful structure–property relationships, thus allowing the prediction of significant features, such as the stability of the A–spacer–B precursor and the rate of B

[a] Dipl.-Chem. A. Alouane, Dr. R. Labruère, S. Dubruille, Dr. F. Schmidt
Institut Curie, Centre de Recherche
26 rue d'Ulm, 75248 Paris (France)
E-mail: raphael.labruere@curie.fr
frederic.schmidt@curie.fr

[b] Dipl.-Chem. A. Alouane, Dr. R. Labruère, S. Dubruille, Dr. F. Schmidt
CNRS, UMR 176, 26 rue d'Ulm, 75248 Paris (France)

[c] Dipl.-Chem. A. Alouane, Dr. R. Labruère, Dr. T. Le Saux, Dr. I. Aujard, Prof. Dr. L. Jullien
Ecole Normale Supérieure, Département de Chimie
UMR CNRS-ENS-UPMC 8640 PASTEUR
24 rue Lhomond, 75231 Paris (France)
E-mail: ludovic.jullien@ens.fr

[d] Dr. T. Le Saux, Prof. Dr. L. Jullien
UPMC Univ. Paris 6, 4 Place Jussieu, 75232 Paris (France)

Supporting information for this article is available on the WWW under <http://dx.doi.org/10.1002/chem.201301298>.

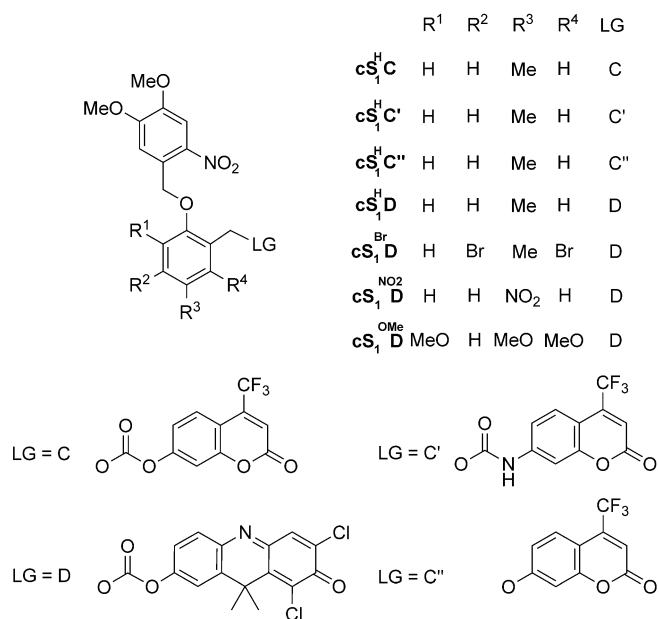
release.^[1a,6] However, these studies used enzymatic/chemical reactions to trigger the disassembly of the spacer, which has limited the temporal resolution of the kinetic analysis to the minute range. In particular, no precise information is presently available for the fastest and highly significant (see above) self-immolative spacers.

Following our recent development of a self-immolative spacer-based caging group that showed fluorescence reporting, we have estimated that photochemical activation could yield significant improvements for investigating the kinetics of self-immolation reactions. Indeed, light gives access to exclusive temporal and spatial resolution, so as to permit the analysis of the kinetics of the fastest processes. Herein, we implemented three procedures that relied on light activation to analyze the kinetics of the disassembly of self-immolative spacer groups at a high temporal resolution of 20 ms. In fact, such a limit is precisely relevant for investigating the behavior of the fastest reported self-immolation processes. Beyond this achievement, we show that those procedures are relevant for analyzing the kinetics of self-immolation processes over a kinetic window that is five orders of magnitude wide (10^{-2} – 10^3 s), which should be favorable for most current applications of self-immolative spacers.

Results and Discussion

Experimental design: Most self-immolative spacer groups are based on phenyl cores that contain a heteroatom that is involved in bond 1, the scission of which causes the cleavage of bond 2 through elimination or cyclization reactions (Scheme 1). We chose to employ a phenol core, along with a quinone-methide-elimination process, because this latter process has been shown to be versatile for releasing two or more leaving groups.^[7] We eventually targeted a series of caged-substituted phenol-containing spacers (cS_1^RLG) with different appended leaving groups (Scheme 2), which were expected to exhibit various disassembly rates after their photoactivation.

To deactivate the precursor, as well as to permit its photoactivation, the phenol oxygen atom was protected with the widely used 4,5-dimethoxy-2-nitrobenzyl caging group. In particular, such 2-nitrobenzyl caging groups have been reported to liberate phenol groups on the millisecond time-scale, which herein makes it possible to analyze self-immolation processes that occur more slowly than within 10 ms.^[8] Various electron-donating (methyl or methoxy) and electron-withdrawing substituents (nitro or bromo) were introduced onto the phenyl ring. Eventually, the benzylic positions of the spacers were bonded to fluorescent reporting moieties through carbonate/carbamate or ether groups. To finely analyze the stoichiometry and the kinetics of the self-immolation of the photoactivated spacers, we chose latent fluorophores for which the emission was quenched and blue-shifted in the caged precursor with respect to in the free state. We retained two coumarins (7-hydroxy-4-(trifluoromethyl)coumarin, **C1**, or 7-amino-4-(trifluoromethyl)cou-

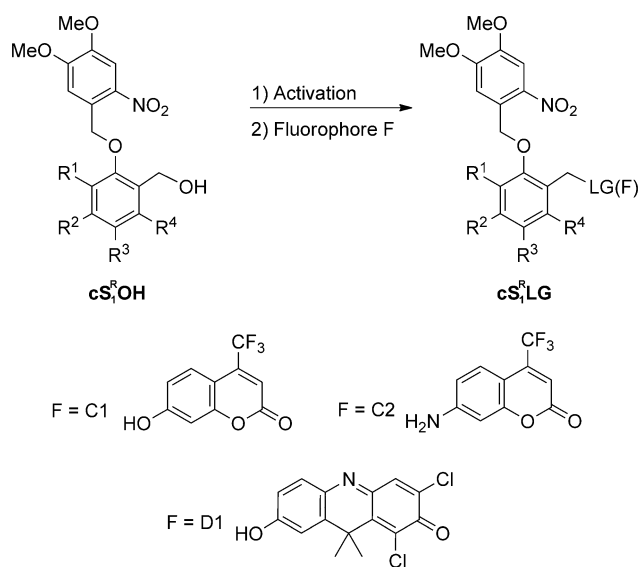


Scheme 2. Caged self-immolative spacers cS_1^RLG .

marin, **C2**) and DDAO (1,3-dichloro-9,9-dimethyl-9*H*-acridin-2(7)-one, **D1**), which respectively exhibited strong emission in the green- and red-light regions, only after liberation of their phenol/aniline groups.^[9]

Synthesis: The caged self-immolative spacers, cS_1^RLG , were synthesized by coupling caged benzyl alcohol modules, cS_1^ROH (see the Supporting Information), with reporting fluorophores after appropriate activation processes (Scheme 3).

Carbonates cS_1^HC and cS_1^RD were synthesized in high overall yields according to literature procedures^[10] in a two-step



Scheme 3. Synthetic pathway for the synthesis of cS_1^RLG .

sequence by using triethylamine in dry THF to couple either coumarin **C1** or DDAO **D1** with the chloroformates that were obtained from the $\text{cS}_1^{\text{R}}\text{OH}$ alcohols in the presence of phosgene. Carbamate $\text{cS}_1^{\text{H}}\text{C}'$ was obtained in 52% yield, according to a closely related procedure that involved carbamylation of anilino-coumarin **C2** with triphosgene, followed by reaction with $\text{cS}_1^{\text{H}}\text{OH}$. Eventually, the synthesis of $\text{cS}_1^{\text{H}}\text{C}''$ was conducted in two steps with an overall yield of 69% by alkylating coumarin **C1** in the presence of K_2CO_3 with the iodo derivative that was obtained after the iodination of $\text{cS}_1^{\text{H}}\text{OH}$.

Photoactivated self-immolation: Stability and photoactivation experiments of $\text{cS}_1^{\text{R}}\text{LG}$ were performed in a mixture of MeCN and 0.1 M Britton–Robinson buffer (1:1, v/v). From the absence of any temporal evolution of the absorption spectrum over the typical 24 h timescale, we concluded that the $\text{cS}_1^{\text{R}}\text{LG}$ molecules were stable in the dark under all of our experimental conditions.

To analyze the self-immolation kinetics of the photoactivated $\text{cS}_1^{\text{R}}\text{LG}$ intermediates, we recorded the temporal evolution of the fluorescence emission from the reporting fluorophore upon submitting solutions of $\text{cS}_1^{\text{R}}\text{LG}$ to continuous illumination at 365 nm to both photoactivate and excite the reporting fluorophores. In a first series of experiments, we illuminated the stirred solutions in a cuvette in a standard spectrofluorimeter, which allowed us to obtain the typical 1 s temporal resolution that is associated with homogeneous mixing. For the fastest systems, we subsequently implemented a stopped-flow mixing technique and performed epifluorescence microscopy, which made it possible to access 40 and 20 ms temporal resolutions, respectively. Our kinetic experiments were performed at three different pH values (to study the incidence of the ionization state of the phenol spacer on the rate of disassembly) within the range 293–318 K (in view of the relevance of self-immulative spacers for biological applications at various temperatures).

Figure 1a shows the temporal evolution of the fluorescence emission, $I_{\text{F}}^{\text{C1}}(t)$, on the release of coumarin **C1** upon continuous illumination of a $(1.0 \pm 0.3) \mu\text{M}$ solution of caged precursor $\text{cS}_1^{\text{H}}\text{C}''$ on the fluorimeter setup. Starting from a nonfluorescent solution of $\text{cS}_1^{\text{H}}\text{C}''$, the fluorescence emission increased, as anticipated from the photoreleasing of coumarin **C1**. The final signal demonstrated the quantitative photo-release of coumarin **C1** from $\text{cS}_1^{\text{H}}\text{C}''$ at all of the investigated temperatures: By using standard solutions of coumarin **C1** for the fluorescence calibration, we derived a value of $(1.5 \pm 0.5) \mu\text{M}$ for the final concentration, CI_{∞} . Similar behaviors were observed for all of the investigated compounds, $\text{cS}_1^{\text{R}}\text{LG}$, thus demonstrating the quantitative release of the reporting fluorophore (**C1**, **C2**, or **D1**) after photoactivation.

A cascade of reactions leads from the photoactivated $\text{cS}_1^{\text{R}}\text{LG}$ precursors to the final reporting fluorophores, **F**. In line with our previous work, for the kinetic analysis, we adopted the shortened scheme as shown in Scheme 4, which retained steps that typically occurred more slowly than on the millisecond timescale (see the Supporting Information).

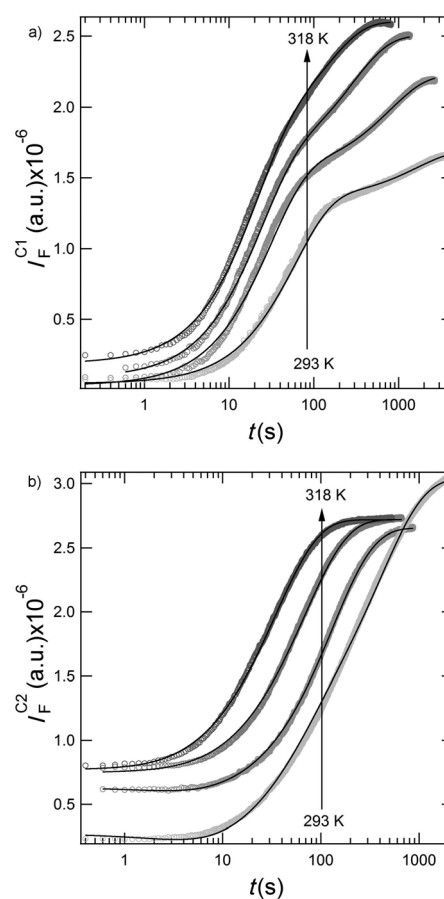
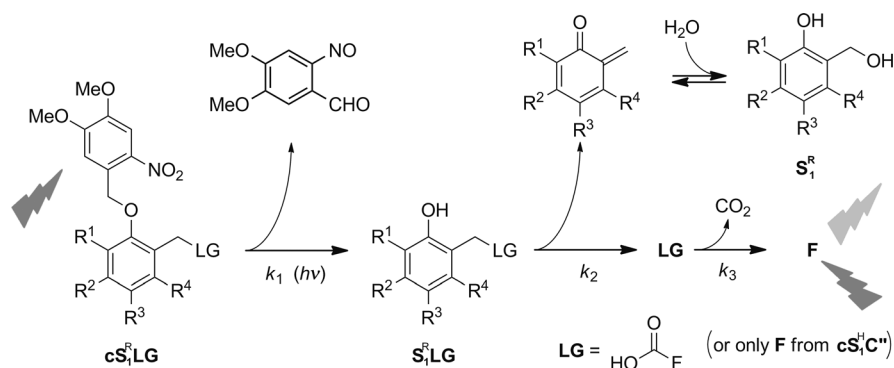


Figure 1. Temporal evolution of the fluorescence emission at $\lambda_{\text{em}} = 500$ nm upon illumination at $\lambda_{\text{exc}} = (365 \pm 25)$ nm of: a) $(1.0 \pm 0.3) \mu\text{M}$ solution of $\text{cS}_1^{\text{H}}\text{C}''$, or b) $(5 \pm 1) \mu\text{M}$ solution of $\text{cS}_1^{\text{H}}\text{C}''$ at 24.5×10^{-9} Ein s^{-1} light intensity at various temperatures. Circles denote the experimental data (293, 303, 310, and 318 K); solid lines show the fits to Equation (13) (a and b at 310 and 318 K) and Equation (45) (b at 293 and 303 K), respectively (see the Supporting Information for all Equations). Solvent: MeCN with 0.1 M Britton–Robinson pH 8 buffer (1:1 v/v).

Illumination of caged precursors $\text{cS}_1^{\text{R}}\text{LG}$ first yielded phenol intermediates $\text{S}_1^{\text{R}}\text{LG}$, which subsequently disassembled into a benzenic core (thereby ultimately yielding structure S_1^{R}), together with a leaving group, **LG**. The reporting coumarin **C1** directly resulted from the disassembly of ether-bounded spacer $\text{S}_1^{\text{H}}\text{C}''$. In the other intermediates, $\text{S}_1^{\text{R}}\text{LG}$, **LG** was a carbonic/carbamic ester, which further decomposed to eventually afford carbon dioxide and the reporting fluorophore, **F**, in a third step. In Scheme 4, rate constant k_1 is associated with photoactivation, whereas rate constants k_2 and k_3 refer to the self-immolation and decarboxylation steps, respectively.

First, we performed the kinetic analysis of the disassembly of compound $\text{S}_1^{\text{H}}\text{C}''$, which only involved two steps. Figure 1a shows that our kinetic model was appropriate for obtaining satisfactory fits at all of the investigated temperatures. Hence, we could determine several parameters: 1) The photoactivation quantum yield, $\phi(365 \text{ nm}) = (72.2 \pm 0.3) \times 10^{-4}$, which was in accordance with reported values for



Scheme 4. Disassembly processes after the photoactivation of caged self-immolative spacer $cS_1^R LG$.

uncaging with the *ortho*-nitrobenzyl group;^[11] 2) the relative brightness of phenol intermediate $S_1^H C''$ with respect to that of coumarin **C1**, 0.4, which was in line with our previous results;^[10] 3) k_2 values, which ranged from $(6.2 \pm 0.3) \times 10^{-4}$ to $(7 \pm 1) \times 10^{-3} s^{-1}$ between 293 and 318 K. Then, these latter values were used to extract the disassembly times of $S_1^H C''$, according to $\tau_d = 1/k_2$, within the range 293–318 K. The results are summarized in Table 1.

Table 1. Disassembly times (τ_d , in s) of the activated self-immolative spacers at various temperatures and pH 8 (unless otherwise indicated).

$cS_1^R LG$	293 K	303 K	310 K	318 K
$cS_1^H C$	(2.3 ± 0.3)	(1.3 ± 0.1)	– ^[a]	– ^[a]
$cS_1^H C'$	(3.7 ± 0.1)	(2.9 ± 0.6)	(2.5 ± 0.1)	(1.2 ± 0.1)
$cS_1^H C''$	(1600 ± 100)	(770 ± 60)	(290 ± 60)	(140 ± 15)
$cS_1^H D$	(6.2 ± 0.9)	(4.9 ± 0.1)	(4.8 ± 0.6)	(4.0 ± 0.3)
$cS_1^{br} D$	–	–	–	–
pH 4	–	(100 ± 5)	–	–
pH 8	(140 ± 15)	(29 ± 1)	(14 ± 4)	(2.6 ± 0.2)
pH 10	–	– ^[a]	–	–
$cS_1^{NO_2} D$	–	–	–	–
pH 4	–	(133 ± 2)	–	–
pH 8	(2.8 ± 0.2)	(2.6 ± 0.4)	(2.5 ± 0.1)	(2.1 ± 0.1)
pH 10	–	$(1.2 \pm 0.1)^{[b]}$	–	–
$cS_1^{OMe} D$	$(0.3 \pm 0.1)^{[b]}$ $(0.7 \pm 0.2)^{[c]}$	$(0.12 \pm 0.02)^{[b]}$	$(0.067 \pm 0.008)^{[b]}$	–

[a] Below the accessible temporal resolution under the measurement conditions. [b] Values extracted from the stopped-flow experiments. [c] Values extracted from the microscopy experiments.

Equipped with these satisfactory results, we performed the more demanding kinetic analysis of the self-immolation of the spacers that contained either carbonate or carbamate groups. Figure 1b shows the temporal evolution of the fluorescence emission, $I_F^{C2}(t)$, on the release of coumarin **C2** upon the continuous illumination of a $(5 \pm 1) \mu M$ solution of caged precursor $cS_1^H C'$ on the fluorimeter setup. Now, relying on a three-step kinetic model (see the Supporting Information), we satisfactorily fitted the experimental data and derived: 1) The photoactivation quantum yield, $\phi(365 \text{ nm}) = (23.3 \pm 0.2) \times 10^{-4}$, which was within the expected range for the *ortho*-nitrobenzyl caging group;^[11] 2) the relative brightnesses of phenol $S_1^H C'$ and of carbamic intermediate

HOCOC**2** with respect to that of coumarin **C2**, 0.4; 3) k_2 values, which ranged from (0.27 ± 0.01) to $(0.8 \pm 0.1) s^{-1}$ between 293 and 318 K; 4) k_3 values, $(2.4 \pm 0.5) \times 10^{-3}$ and $(8 \pm 1) \times 10^{-3} s^{-1}$ at 293 and 303 K respectively,^[12] in agreement with reported values for the decarboxylation of carbamic acid.^[13]

Then, the corresponding experiments and analyses were performed for the caged self-immolative spacers that contained a carbonate group (for an exhaustive report of the experimental data, see the Supporting Information). In those cases, we could notably use a condensed kinetic model, which focused on the two first steps shown in Scheme 4, because the final decarboxylation step was faster (below the millisecond timescale^[14]) than the temporal resolution of our fluorescence-acquisition setup. Again, the extracted values of the photoactivation quantum yields, $\phi(365 \text{ nm})$, were in line with literature expectations^[11] and we could retrieve the disassembly times according to $\tau_d = 1/k_2$ (Table 1).

During the course of the preceding experiments, we noticed that the two-step kinetic model was poorly reliable in the case of the $cS_1^{OMe} D$ caged spacer. Indeed, we successfully accounted for the experimental behavior by using a one-step kinetic model (see the Supporting Information, Figure S11a), which suggested that the self-immolation step occurred faster than the temporal resolution of our experimental design.^[10,15] To gain further insight into the self-immolation rate constant of $cS_1^{OMe} D$, we first equipped our fluorimeter with a stopped-flow accessory, thus allowing us to achieve a temporal resolution of 40 ms. Indeed, we have now reliably analyzed the results of the illumination experiments by using the two-step kinetic model (see the Supporting Information, Figure S11b), which yielded $\tau_d(S_1^{OMe} D)$ values in the range 70–300 ms (Table 1).

To confirm the reliability of our estimates, we devised an alternative experiment that provided us with a temporal resolution of down to 20 ms (limited by the acquisition frequency of our camera). An $80 \mu M$ solution of $cS_1^{OMe} D$ was introduced into multiple micrometric cavities of a PDMS microfluidic device, which were submitted to homogeneous illumination at 360 nm and optical recording on an epifluorescence setup (Figure 2a and b and the file Movie.avi^[23] in the Supporting Information).^[10,16] The temporal evolution of the fluorescence signal from several neighboring cavities is shown in Figure 2c, together with the fit that was obtained by using the two-step kinetic model. Thus, we extracted $\tau_d(S_1^{OMe} D) = 700 \text{ ms}$ at 293 K, which was in reasonable agreement with the result that was obtained by stopped-flow analysis.

Discussion

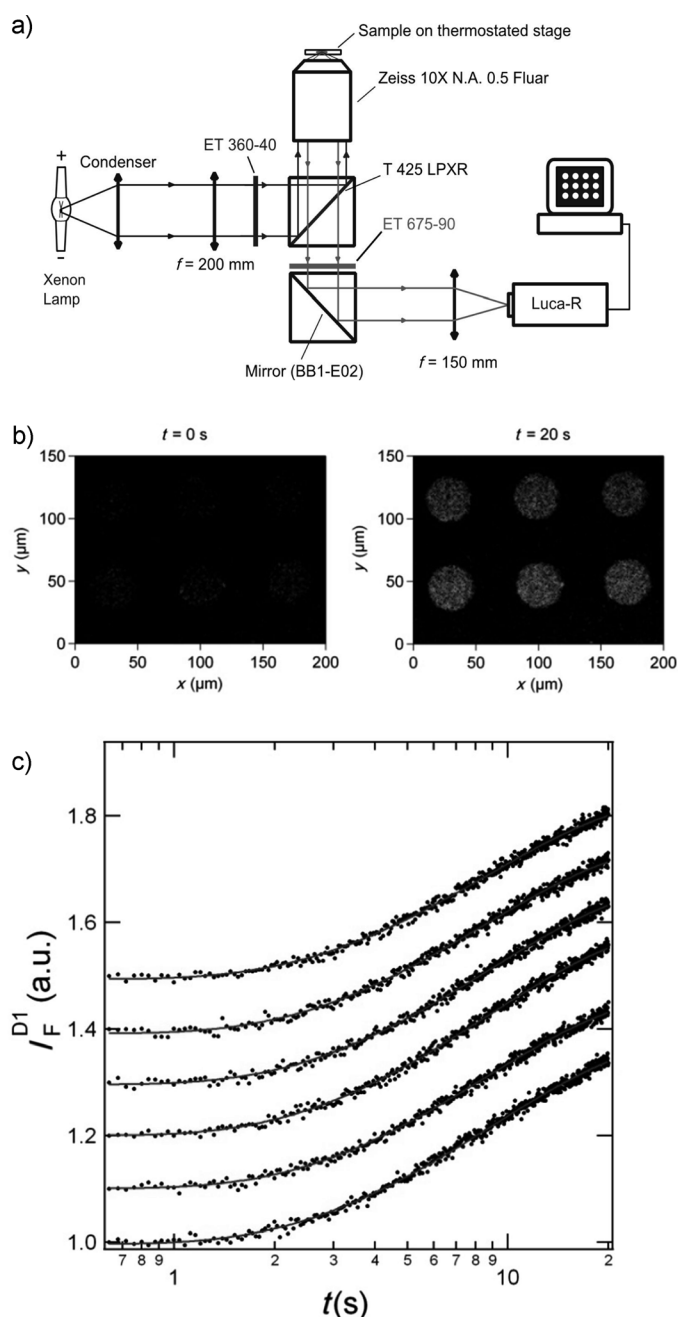


Figure 2. Disassembly processes after the photoactivation of caged self-immolative spacer $\text{cS}_1^{\text{Me}}\text{LG}$. a) Schematic representation of the epifluorescence microscope. b) Micrographs ($\lambda_{\text{em}} = (675 \pm 45)$ nm) of a polydimethylsiloxane (PDMS) microfluidic device that initially contained (80 ± 5) μm $\text{cS}_1^{\text{OMe}}\text{D}$ before ($t = 0$ s) and after ($t = 20$ s) photoactivation at $\lambda_{\text{exc}} = (360 \pm 20)$ nm with 2.5×10^{-3} $\text{Ein s}^{-1} \text{m}^{-2}$ light intensity. c) Temporal evolution of the fluorescence emission, $I_F^{\text{Cl}}(t)$, from six neighboring $\text{cS}_1^{\text{OMe}}\text{D}$ -containing wells (a vertical offset has been added for comparison). Circles denote the experimental data; solid lines show the fits to Equation (46), thus yielding $\langle k_1 \rangle = (0.116 \pm 0.003) \text{ s}^{-1}$ and $\langle k_2 \rangle = (1.11 \pm 0.07) \text{ s}^{-1}$. Solvent: MeCN with 0.1 M Britton–Robinson pH 8 buffer (1:1, v/v), $T = 293$ K.

This investigation shows that this series of self-immolative spacer groups can be tailored to release a substrate from the 10^{-1} to the 10^3 s timescales. These results are in good agreement with previously reported structure–property relationships,^[1a] but the precise determination of the associated kinetic information is now possible. The elimination of quinone methide is typically $\times 10^3$ -times slower when the reporting phenol fluorophore is directly grafted on through an ether bond rather than through a carbonate or carbamate linkage (cf. $\text{cS}_1^{\text{H}}\text{C}''$ with $\text{cS}_1^{\text{H}}\text{C}$, $\text{cS}_1^{\text{H}}\text{D}$, and $\text{cS}_1^{\text{H}}\text{C}'$).^[17] Notably, the carbonyl moiety acts as an efficient uncoupling fragment; despite major differences between the nucleofugacity of structures **C1**, **D1**, and **C2**, the elimination of quinone methide occurs at similar timescales in $\text{cS}_1^{\text{H}}\text{C}$, $\text{cS}_1^{\text{H}}\text{D}$, and $\text{cS}_1^{\text{H}}\text{C}'$. However, the slow decarboxylation of the carbamic acid intermediate postpones the release of the final substrate in carbamate $\text{cS}_1^{\text{H}}\text{C}'$. Phenol ionization typically accelerates the disassembly of the spacer by a factor of $\times 10^2$ (cf. $\text{cS}_1^{\text{NO}_2}\text{D}$ and $\text{cS}_1^{\text{Br}}\text{D}$ in the range pH 4–10; the associated phenols exhibit $\text{p}K$ 8.1 and 9.5, respectively; see the Supporting Information). Retaining the nonionized phenol state to analyze the influence of the substitution pattern, we relied on data that were acquired at pH 8 for $\text{cS}_1^{\text{H}}\text{D}$ and $\text{cS}_1^{\text{NO}_2}\text{D}$ (with associated phenols exhibiting $\text{p}K$ 11.6 and 11.7) and pH 4 for $\text{cS}_1^{\text{Br}}\text{D}$ and $\text{cS}_1^{\text{NO}_2}\text{D}$. Hence, in line with the development of a positive charge on the exocyclic methylene during the elimination of quinone methide,^[6] we observed that appending electron-donating groups onto the phenyl core accelerated the disassembly of the spacer. The disassembly time typically decreased by a factor of 20 on replacing an appending inductive electron-withdrawing group ($m\text{-NO}_2$ or $o,p\text{-Br}$ in $\text{cS}_1^{\text{NO}_2}\text{D}$ and $\text{cS}_1^{\text{Br}}\text{D}$) by an inductive electron-donating group ($m\text{-Me}$ in $\text{cS}_1^{\text{H}}\text{D}$). Another drop by a factor of 50 was observed upon replacing an inductive electron-donating group ($m\text{-Me}$ in $\text{cS}_1^{\text{H}}\text{D}$) by a conjugated strongly mesomeric electron-donating group ($o\text{-OMe}$ in $\text{cS}_1^{\text{OMe}}\text{D}$). Eventually, the disassembly time is typically expected to drop by a factor of 10 upon increasing the temperature by 25 K from room temperature.

One should emphasize the relevance of this photoactivation approach for reliably extracting the kinetic parameters that are associated with the self-immolation process over a broad kinetic window. In particular, whereas the fastest self-immolations have been reported to occur within a few seconds,^[17a,18] this investigation is the first to show that those self-immolation events occur precisely on the 100 ms timescale. For instance, this information will be significant for choosing the relevant concentration of a prodrug to circumvent drug activation to the close perimeter of an activating enzyme.^[19] Furthermore, this approach will permit access to even much faster timescales. Indeed, whereas temporal resolution of the cuvette experiments are ultimately limited by the homogenization timescales (at most 40 ms with our stopped-flow equipment), this procedure, which relies on homogenous illumination with an epifluorescence microscope

setup, will be only limited by the acquisition frequency of the camera. Hence, it should easily yield information on the ms timescale with a fast camera.

Conclusion

We have introduced and implemented three procedures that rely on light activation to accurately analyze the disassembly kinetics of a collection of self-immolative spacer groups over a wide kinetic window (10^{-2} – 10^3 s). Our results are relevant for deriving quantitative structure–property relationships, which should be especially significant in the context of prodrugs. In particular, we have been able to access a temporal resolution of 20 ms, which made it possible to measure the shortest disassembly time ever reported for an activated self-immolative spacer.

Experimental Section

Synthesis: The commercially available chemicals were used without further purification. Anhydrous solvents were freshly distilled before use. Low-actinic glassware was used for all experiments with compounds that contained nitroveratryl moieties. Column chromatography was performed on Merck silica gel 60 (0.040–0.063 mm). Analytical and thin layer chromatography (TLC) was performed on Merck silica gel 60 F-254 precoated plates; detection was performed by using UV light ($\lambda=254$ nm). NMR spectra were recorded on an AC Bruker spectrometer at 300 MHz (for ^1H nuclei) and 75 MHz (for ^{13}C nuclei). Coupling constants (J) are in Hz. HPLC analyses and purifications of the final caged species were performed on a Waters system with a Wdelta 600 pump and a PDA 996 UV detector at $\lambda=245$ nm (analytical HPLC: X-Terra Waters MS C18 column, 150 mm \times 4.6 mm, 5 mm, flow rate: 1 mL min^{-1} ; preparative HPLC: X-Terra Waters Prep MS C18 column, 150 mm \times 19 mm, 5 mm, flow rate: 10 mL min^{-1} ; elution with MeCN/water mixtures). For information on the syntheses of the intermediate benzylic alcohols, **cs^ROH**, see the Supporting Information.

General procedure for the preparation of caged self-immolative spacers that contain carbonic leaving groups: To a solution of the desired benzylic alcohol intermediate (**cs^ROH**, 0.01 mmol) in anhydrous THF (10 mL) at 0°C under an Ar atmosphere was quickly added a 20% solution of phosgene in toluene (25 μL , 0.05 mmol) by using a syringe. The mixture was stirred at RT for 2 h and Ar gas was then bubbled through the solution for 15 min to remove any unreacted phosgene. The purged solution was added dropwise to a solution of Et₃N (8 μL , 0.06 mmol) and the desired reporter, 7-hydroxy-4-(trifluoromethyl)-2*H*-chromen-2-one or DDAO (0.02 mmol), in anhydrous THF (10 mL) and the mixture was cooled to 0°C and stirred for 15 min. The resulting suspension was diluted with CH₂Cl₂ (10 mL) and a 1 M aqueous solution of HCl (20 mL) was added. The organic phase was separated, dried over MgSO₄, and evaporated under reduced pressure. The crude product was purified by preparative HPLC (MeCN/water 90:10 v/v).

cs^HC: White solid (40% yield); ^1H NMR (300 MHz, CDCl₃, 25°C): $\delta=7.79$ (s, 1H), 7.73 (d, $J=9$ Hz, 1H), 7.45 (s, 1H), 7.27 (d, $J=2$ Hz, 1H), 7.26 (d, $J=2$ Hz, 1H), 7.19 (dd, $J=9, 2$ Hz, 1H), 7.18 (dd, $J=8, 2$ Hz, 1H), 6.92 (d, $J=8$ Hz, 1H), 6.78 (s, 1H), 5.54 (s, 2H), 5.46 (s, 2H), 3.98 (s, 3H), 3.96 (s, 3H), 2.33 ppm (s, 3H); ^{13}C NMR (75 MHz, CDCl₃, 25°C): $\delta=158.2, 154.9, 154.0, 153.9, 152.4, 147.8, 138.9, 131.7, 131.1, 130.6, 129.3, 129.0, 126.3, 122.2, 118.1, 115.4, 112.0, 111.3, 110.3, 109.3, 107.8, 67.0, 56.3, 20.3$ ppm; LRMS (ES+): m/z : 612 [$M+\text{Na}$]⁺; HRMS (ES+): m/z calcd for C₂₈H₂₂F₃NNaO₁₀: 612.1088 [$M+\text{Na}$]⁺; found: 612.1081.

cs^HD: Yellow solid (61% yield); ^1H NMR (300 MHz, CDCl₃, 25°C): $\delta=7.78$ (s, 1H), 7.65 (d, $J=9$ Hz, 1H), 7.63 (s, 1H), 7.48 (s, 1H), 7.29 (d, $J=2$ Hz, 1H), 7.28 (d, $J=2$ Hz, 1H), 7.18 (dd, $J=9, 2$ Hz, 1H), 7.17 (dd, $J=8, 2$ Hz, 1H), 6.91 (d, $J=8$ Hz, 1H), 5.55 (s, 2H), 5.45 (s, 2H), 3.97 (s, 6H), 2.33 (s, 3H), 1.86 ppm (s, 6H); ^{13}C NMR (75 MHz, CDCl₃, 25°C): $\delta=173.1, 154.3, 154.1, 153.4, 153.0, 150.0, 147.8, 140.2, 139.5, 139.4, 138.9, 138.6, 137.5, 135.7, 133.1, 131.8, 131.2, 130.8, 129.3, 122.5, 120.8, 119.1, 112.1, 109.3, 107.9, 67.1, 66.9, 56.5, 56.4, 39.1, 26.6, 20.4$ ppm; LRMS (ES+): m/z : 689 [$M+\text{Na}$]⁺; HRMS (ES+): m/z calcd for C₃₃H₂₀Cl₂N₂O₉: 667.1244 [$M+\text{H}$]⁺; found: 667.1238.

cs^RD: Yellow solid (55% yield); ^1H NMR (300 MHz, CDCl₃, 25°C): $\delta=7.79$ (s, 1H), 7.65 (d, $J=9$ Hz, 1H), 7.63 (s, 1H), 7.35 (s, 1H), 7.29 (d, $J=2$ Hz, 1H), 7.24 (s, 1H), 7.17 (dd, $J=9, 2$ Hz, 1H), 5.67 (s, 2H), 5.54 (s, 2H), 3.97 (s, 3H), 3.95 (s, 3H), 2.60 (s, 3H), 1.85 ppm (s, 6H); ^{13}C NMR (75 MHz, CDCl₃, 25°C): $\delta=173.1, 155.5, 154.1, 153.3, 152.8, 150.0, 148.2, 140.1, 139.4, 139.1, 138.6, 137.5, 135.7, 133.1, 131.4, 129.9, 127.7, 126.9, 122.6, 120.6, 119.1, 116.2, 109.3, 108.2, 68.1, 66.1, 56.6, 56.4, 39.1, 26.6, 23.9$ ppm; LRMS (ES+): m/z : 825 [$M+\text{H}$]⁺; HRMS (ES+): m/z calcd for C₃₃H₂₇Br₂Cl₂N₂O₉: 824.9440 [$M+\text{H}$]⁺; found: 824.9435.

cs^NO₂D: Yellow solid (85% yield); ^1H NMR (300 MHz, CDCl₃, 25°C): $\delta=8.43$ (d, $J=9$ Hz, 1H), 8.33 (dd, $J=9, 3$ Hz, 1H), 7.81 (s, 1H), 7.67 (d, $J=9$ Hz, 1H), 7.64 (s, 1H), 7.36 (s, 1H), 7.31 (d, $J=2$ Hz, 1H), 7.19 (dd, $J=9, 2$ Hz, 1H), 7.14 (d, $J=9$ Hz, 1H), 5.69 (s, 2H), 5.50 (s, 2H), 3.99 (s, 6H), 1.87 ppm (s, 6H); ^{13}C NMR (75 MHz, CDCl₃, 25°C): $\delta=173.1, 160.7, 154.2, 153.1, 152.8, 150.1, 148.4, 141.8, 140.1, 139.6, 139.4, 139.2, 138.7, 137.5, 135.7, 133.2, 126.9, 126.8, 126.1, 124.1, 120.6, 119.1, 111.8, 109.2, 108.2, 67.9, 65.3, 56.6, 56.5, 39.1, 26.6$ ppm; LRMS (ES+): m/z : 720 [$M+\text{Na}$]⁺; HRMS (ES+): m/z calcd for C₃₂H₂₆Cl₂N₂O₁₁: 698.0938 [$M+\text{H}$]⁺; found: 698.0953.

cs¹MeD: Yellow solid (82% yield); ^1H NMR (300 MHz, CDCl₃, 25°C): $\delta=7.70$ (s, 1H), 7.63 (s, 1H), 7.62 (s, 1H), 7.60 (d, $J=9$ Hz, 1H), 7.23 (d, $J=2$ Hz, 1H), 7.06 (dd, $J=9, 2$ Hz, 1H), 6.67 (s, 1H), 5.44 (s, 2H), 5.43 (s, 2H), 4.00 (s, 3H), 3.93 (s, 3H), 3.91 (s, 3H), 3.87 (s, 3H), 3.86 (s, 3H), 1.86 ppm (s, 6H); ^{13}C NMR (75 MHz, CDCl₃, 25°C): $\delta=173.5, 154.3, 153.8, 153.1, 150.3, 149.9, 149.4, 148.0, 142.3, 140.6, 139.8, 139.1, 138.9, 136.0, 133.4, 130.8, 122.7, 121.0, 119.5, 109.9, 108.0, 100.5, 72.6, 62.2, 61.7, 56.9, 56.7, 39.5, 26.9$ ppm; LRMS (ES+): m/z : 743 [$M+\text{H}$]⁺; HRMS (ES+): m/z calcd for C₃₅H₃₃Cl₂N₂O₁₂: 743.1405 [$M+\text{H}$]⁺; found: 743.1400.

cs^HC: To a solution of 7-amino-4-(trifluoromethyl)-2*H*-chromen-2-one (10 mg, 0.04 mmol) and Et₃N (24 μL , 0.08 mmol) in anhydrous CH₂Cl₂ (1 mL) at 0°C under an Ar atmosphere was added a solution of triphosgene (15 mg, 0.05 mmol) in anhydrous CH₂Cl₂ (1 mL). The solution was stirred at 0°C for 2 h, a solution of alcohol **cs^HOH** (14 mg, 0.04 mmol) in anhydrous CH₂Cl₂ (2 mL) was slowly added at 0°C, and the reaction mixture was stirred for a further 2 h at RT. The resulting suspension was filtered and the crude precipitate was purified by preparative HPLC (A/B, 90:10) to afford compound **cs^HC** as a white solid (12 mg, 52% yield). ^1H NMR (300 MHz, [D₇]DMF, 25°C): $\delta=10.61$ (s, 1H), 7.94 (s, 1H), 7.93 (d, $J=2$ Hz, 1H), 7.87 (d, $J=9$ Hz, 1H), 7.71 (dd, $J=8, 2$ Hz, 1H), 7.70 (s, 1H), 7.49 (d, $J=2$ Hz, 1H), 7.41 (dd, $J=9, 2$ Hz, 1H), 7.31 (d, $J=8$ Hz, 1H), 7.04 (s, 1H), 5.68 (s, 2H), 5.52 (s, 2H), 4.16 (s, 3H), 4.11 (s, 3H), 2.48 ppm (s, 3H); LRMS (ES+): m/z : 606 [$M+\text{NH}_4$]⁺; HRMS (ES+): m/z calcd for C₂₈H₂₇F₃N₃O₉: 606.1693 [$M+\text{NH}_4$]⁺; found: 606.1688.

cs^HC: To a stirring solution of PPh₃ (60 mg, 0.23 mmol), imidazole (16 mg, 0.23 mmol), and iodine (58 mg, 0.23 mmol) in anhydrous CH₂Cl₂ (10 mL) was added alcohol **cs^HOH** (87 mg, 0.15 mmol). The resulting mixture was stirred at RT for 4 h and filtered to remove the precipitate. A saturated aqueous solution of Na₂S₂O₃ (20 mL) and CH₂Cl₂ (30 mL) were successively added to the filtrate. The organic phase was separated, dried over MgSO₄, and evaporated under reduced pressure. The crude residue was purified by column chromatography on silica gel (cyclohexane/EtOAc, 8:2 v/v) to afford 1-((2-(iodomethyl)-4-methylphenoxy)methyl)-4,5-dimethoxy-2-nitrobenzene as a white solid (50 mg, 75% yield). ^1H NMR (300 MHz, CDCl₃, 25°C): $\delta=7.79$ (s, 1H), 7.60 (s, 1H), 7.15 (s, 1H), 7.07 (d, $J=8$ Hz, 1H), 6.80 (d, $J=8$ Hz, 1H), 5.54 (s, 2H), 4.56 (s, 2H), 4.07 (s, 3H), 3.98 (s, 3H), 2.28 ppm (s, 3H); ^{13}C NMR (75 MHz, CDCl₃, 25°C): $\delta=154.6, 153.9, 148.2, 139.1, 131.1, 130.8, 129.9, 127.4,$

112.6, 109.9, 108.3, 67.3, 57.8, 56.8, 20.8, 2.4 ppm; LRMS (ES+): m/z : 466 [M+Na]⁺; HRMS (ES+): m/z calcd for C₁₇H₂₂IN₂O₅: 461.0567 [M+NH₄]⁺; found: 461.0570.

To a stirring solution of 1-((2-(iodomethyl)-4-methylphenoxy)methyl)-4,5-dimethoxy-2-nitrobenzene (30 mg, 0.07 mmol) in anhydrous DMF (10 mL) was added K₂CO₃ (14 mg, 0.1 mmol) and 7-hydroxy-4-(trifluoromethyl)-2H-chromen-2-one (16 mg, 0.07 mmol). The mixture was stirred at RT for 2 h and then CH₂Cl₂ (20 mL) and water (20 mL) were added. The organic phase was separated, dried over MgSO₄, and evaporated under reduced pressure. The crude residue was purified by column chromatography on silica gel (cyclohexane/EtOAc, 8:2 v/v) to afford compound **CS^HC^W** as a white solid (35 mg, 92% yield). ¹H NMR (300 MHz, CDCl₃, 25 °C): δ = 7.75 (s, 1H), 7.62 (d, J = 9 Hz, 1H), 7.31 (s, 1H), 7.25 (d, J = 2 Hz, 1H), 7.15 (dd, J = 8, 2 Hz, 1H), 6.99 (dd, J = 9, 2 Hz, 1H), 6.98 (d, J = 2 Hz, 1H), 6.91 (d, J = 8 Hz, 1H), 6.62 (s, 1H), 5.51 (s, 2H), 5.25 (s, 2H), 3.96 (s, 3H), 3.76 (s, 3H), 2.32 ppm (s, 3H); ¹³C NMR (75 MHz, CDCl₃, 25 °C): δ = 162.8, 159.2, 156.3, 153.9, 147.9, 139.2, 131.1, 130.6, 128.9, 126.4, 123.4, 113.9, 112.5, 109.3, 108.1, 107.1, 102.2, 67.6, 66.5, 56.4, 56.1, 20.5 ppm; LRMS (ES+): m/z : 568 [M+Na]⁺; HRMS (ES+): m/z calcd for C₂₇H₂₂F₃NNaO₈: 568.1189 [M+Na]⁺; found: 568.1183.

Analytical solutions: All of the experiments were performed in MeCN with 0.1 M Britton–Robinson buffer (1:1, v/v).^[20] All of the solutions were prepared by using water that was purified on a Direct-Q 5 system (Millipore, Billerica, MA).

pH measurements: pH measurements were performed on a Standard pH meter PHM210 Radiometer Analytical (calibrated with aqueous buffers at pH 4 and 7 or 10) with a Crison 5208 Electrode (Barcelona, Spain), which was accurate over the pH range 0–14.

UV/Vis absorption spectroscopy: UV/Vis absorption spectra were recorded in 1 cm × 1 cm quartz cuvettes (Hellma) on a diode-array UV/Vis spectrophotometer (Evolution Array, Thermo Scientific) at 298 K. Molar absorption coefficients were extracted whilst checking the validity of the Beer–Lambert law.

The evolution of the absorbance as a function of pH value were analyzed by using the SPECFIT/32 Global Analysis System (version 3.0 for 32-bit Windows systems) to extract the pK values of the core phenol groups of the self-immolative spacers (see the Supporting Information).^[21]

Steady-state fluorescence emission spectroscopy: Corrected fluorescence spectra upon one-photon excitation were recorded on a Photon Technology International QuantaMaster QM-1 spectrofluorimeter (PTI, Monmouth Junction, NJ) that was equipped with a Peltier cell-holder (TLC50, Quantum Northwest, Shoreline, WA). Solutions for the fluorescence measurements were adjusted to concentrations such that the absorption maximum was about 0.15 at the excitation wavelength.

Irradiation experiments: Three different procedures were used to perform the one-photon irradiation, that is, on a spectrofluorimeter (with or without stopped-flow) or on an epifluorescence microscope.

On the spectrofluorimeter, irradiations were performed on 400 μL samples in 0.2 × 1 cm² quartz fluorescence cuvettes (Hellma) by using a filtered 75 W xenon lamp at several slit widths under constant stirring. The incident-light intensities were calibrated by using α-(4-dimethylamino-phenyl)-*N*-phenyltrone actinometer, as reported previously.^[22] Typical integral incident-light intensities were within the range 1 × 10⁻⁹ Ein s⁻¹.

On the epifluorescence microscope, solutions were introduced in 40 × 10 μm² (Ø × h) cylindrical microcuvettes that were generated in a PDMS stamp after standard photolithography. The PDMS microdevice was fixed onto the microscope stage and submitted to irradiations with a 100 W xenon lamp (LOT-Oriel, Palaiseau, France) that was equipped with an excitation filter (360 ± 20) nm and a dichroic mirror (T425 LPXR, Chroma Technology, Bellows Falls, VT, USA); the fluorescence emission was recorded by using a × 10 objective (Fluor NA 0.5; Zeiss, Le Pecq, France), which was mounted onto a home-built microscope that was equipped with a Luca-R CCD camera (Andor Technology, Belfast, UK), at (675 ± 45) nm (Chroma Technology, Bellows Falls, VT, USA). 3000 Images were recorded at 25 Hz (exposure time: 39 ms). The signal was averaged within each well over 20 × 20 μm² square areas. Photon-flux

densities were recorded on a Nova II power meter (Laser Measurement Instruments). Typical light fluxes were within the range 2.5 × 10⁻³ Ein s⁻¹ m⁻².

Acknowledgements

This work was supported by the ANR PCV 2008 (Proteophane) and the ANR Blanc 2010 (Kituse). We thank Katherine J. Silvestre and Géraldine Hallais for providing technical assistance.

- [1] a) C. A. Blencowe, A. T. Russell, F. Greco, W. Hayes, D. W. Thornthwaite, *Polym. Chem.* **2011**, *2*, 773–790; b) A. D. Wong, M. A. DeWit, E. R. Gillies, *Adv. Drug Delivery Rev.* **2012**, *64*, 1031–1045.
- [2] P. L. Carl, P. K. Chakravarty, J. A. Katzenellenbogen, *J. Med. Chem.* **1981**, *24*, 479–480.
- [3] a) J. C. Florent, X. Dong, G. Gaudel, S. Mitaku, C. Monneret, J. P. Gesson, J. C. Jacquesy, M. Mondon, B. Renoux, S. Andrianomenjanahary, S. Michel, M. Koch, F. Tillequin, M. Gerken, J. Czech, R. Straub, K. Bosslet, *J. Med. Chem.* **1998**, *41*, 3572–3581; b) B. E. Toki, C. G. Cerveny, A. F. Wahl, P. D. Senter, *J. Org. Chem.* **2002**, *67*, 1866–1872; c) M. Shamis, H. N. Lode, D. Shabat, *J. Am. Chem. Soc.* **2004**, *126*, 1726–1731; d) R. J. Amir, M. Popkov, R. A. Lerner, C. F. Barbas III, D. Shabat, *Angew. Chem.* **2005**, *117*, 4452–4455; *Angew. Chem. Int. Ed.* **2005**, *44*, 4378–4381; e) A. Gopin, S. Ebner, B. Attali, D. Shabat, *Bioconjugate Chem.* **2006**, *17*, 1432–1440.
- [4] a) N. H. Ho, R. Weissleder, C. H. Tung, *ChemBioChem* **2007**, *8*, 560–566; b) T. Chauvin, P. Durand, M. Bernier, H. Meudal, B. T. Doan, F. Noury, B. Badet, J. C. Beloeil, E. Tóth, *Angew. Chem.* **2008**, *120*, 4442–4444; *Angew. Chem. Int. Ed.* **2008**, *47*, 4370–4372; c) E. Sella, D. Shabat, *J. Am. Chem. Soc.* **2009**, *131*, 9934–9936; d) G. C. van de Bittner, E. A. Dubikovskaya, C. R. Bertozzi, C. J. Chang, *Proc. Natl. Acad. Sci. USA* **2010**, *107*, 21316–21321; e) M. S. Baker, S. T. Phillips, *J. Am. Chem. Soc.* **2011**, *133*, 5170–5173; f) G. G. Lewis, M. J. Ditucci, S. T. Phillips, *Angew. Chem.* **2012**, *124*, 12879–12882; *Angew. Chem. Int. Ed.* **2012**, *51*, 12707–12710; g) H. Xie, J. Mire, Y. Kong, M. Chang, H. A. Hassounah, C. N. Thornton, J. C. Sacchettini, J. D. Cirillo, J. Rao, *Nat. Chem.* **2012**, *4*, 802–809; h) O. Redy, D. Shabat, *J. Controlled Release* **2012**, *164*, 276–282; i) K. Yeung, K. M. Schmid, S. T. Phillips, *Chem. Commun.* **2013**, *49*, 394–396.
- [5] Q. T. Nguyen, E. S. Olson, T. A. Aguilera, T. Jiang, M. Scadeng, L. G. Ellies, R. Y. Tsien, *Proc. Natl. Acad. Sci. USA* **2010**, *107*, 4317–4322.
- [6] a) M. P. Hay, B. M. Sykes, W. A. Denny, C. J. O'Connor, *J. Chem. Soc. Perkin Trans. 1* **1999**, *19*, 2759–2770; b) E. E. Weinert, R. Dondi, S. Colloredo-Melz, K. N. Frankenfield, C. H. Mitchell, M. Freccero, S. E. Rokita, *J. Am. Chem. Soc.* **2006**, *128*, 11940–11947; c) K. M. Schmid, L. Jensen, S. T. Phillips, *J. Org. Chem.* **2012**, *77*, 4363–4374; d) R. A. Mosey, P. E. Floreancig, *Org. Biomol. Chem.* **2012**, *10*, 7980–7985.
- [7] a) F. M. H. de Groot, C. Albrecht, R. Koekkoek, P. H. Beusker, H. W. Scheeren, *Angew. Chem.* **2003**, *115*, 4628–4632; *Angew. Chem. Int. Ed.* **2003**, *42*, 4490–4494; b) R. J. Amir, N. Pessah, M. Shamis, D. Shabat, *Angew. Chem.* **2003**, *115*, 4632–4637; *Angew. Chem. Int. Ed.* **2003**, *42*, 4494–4499; c) M. L. Szalai, R. M. Kevitch, D. V. McGrath, *J. Am. Chem. Soc.* **2003**, *125*, 15688–15689.
- [8] R. Jasuja, J. Keyoung, G. P. Reid, D. R. Trentham, S. Khan, *Biophys. J.* **1999**, *76*, 1706–1719.
- [9] a) J. T. M. Buters, C. D. Schiller, R. C. Chou, *Biochem. Pharmacol.* **1993**, *46*, 1577–1584; b) D. Warther, F. Bolze, J. Lonéard, S. Gug, A. Specht, D. Puliti, X.-H. Sun, P. Kessler, Y. Lutz, J.-L. Vonesch, B. Winsor, J.-F. Nicoud, M. Goeldner, *J. Am. Chem. Soc.* **2010**, *132*, 2585–2590; c) H.-J. Jin, J. Lu, X. Wu, *Bioorg. Med. Chem.* **2012**, *20*, 3465–3469.

- [10] R. Labruère, A. Alouane, T. Le Saux, I. Aujard, P. Pelupessy, A. Gautier, S. Dubruille, F. Schmidt, L. Jullien, *Angew. Chem.* **2012**, *124*, 9478–9481; *Angew. Chem. Int. Ed.* **2012**, *51*, 9344–9347.
- [11] I. Aujard, C. Benbrahim, M. Gouget, O. Ruel, J.-B. Baudin, P. Neveu, L. Jullien, *Chem. Eur. J.* **2006**, *12*, 6865–6879.
- [12] The relaxation times that were associated with the photoactivation and decarboxylation steps could not be discriminated at 310 and 318 K; at the corresponding temperatures, $k_1 \approx k_3$.
- [13] a) M. Caplow, *J. Am. Chem. Soc.* **1968**, *90*, 6795–6803; b) S. L. Johnson, D. L. Morrison, *J. Am. Chem. Soc.* **1972**, *94*, 1323–1334.
- [14] a) C. K. Sauer, W. P. Jencks, S. Groh, *J. Am. Chem. Soc.* **1975**, *97*, 5546–5553; b) J. Zhao, T. D. Gover, S. Muralidharan, D. A. Auston, D. Weinreich, J. P. Y. Kao, *Biochemistry* **2006**, *45*, 4915–4926.
- [15] a) N. Gagey, P. Neveu, L. Jullien, *Angew. Chem.* **2007**, *119*, 2519–2521; *Angew. Chem. Int. Ed.* **2007**, *46*, 2467–2469; b) N. Gagey, P. Neveu, C. Benbrahim, B. Goetz, I. Aujard, J.-B. Baudin, L. Jullien, *J. Am. Chem. Soc.* **2007**, *129*, 9986–9998; c) N. Gagey, M. Emond, P. Neveu, C. Benbrahim, B. Goetz, I. Aujard, J.-B. Baudin, L. Jullien, *Org. Lett.* **2008**, *10*, 2341–2344.
- [16] a) K. Zrelli, T. Barilero, E. Cavatore, H. Berthoumieux, T. Le Saux, V. Croquette, A. Lemarchand, C. Gosse, L. Jullien, *Anal. Chem.* **2011**, *83*, 2476–2484; b) T. Barilero, T. Le Saux, C. Gosse, L. Jullien, *Anal. Chem.* **2009**, *81*, 7988–8000.
- [17] a) H. Y. Lee, X. Jiang, D. Lee, *Org. Lett.* **2009**, *11*, 2065–2068; b) J. L. Major Jourden, K. B. Daniel, S. M. Cohen, *Chem. Commun.* **2011**, *47*, 7968–7970.
- [18] R. M. Kevitch, C. S. Shanahan, D. V. McGrath, *New J. Chem.* **2012**, *36*, 492–505.
- [19] J. D. Varner, *Syst. Biol.* **2005**, *152*, 291–302.
- [20] C. Frugoni, *Gazz. Chim. Ital.* **1957**, *87*, 403–407.
- [21] a) H. Gampp, M. Maeder, C. J. Meyer, A. D. Zuberbühler, *Talanta* **1985**, *32*, 95–101; b) H. Gampp, M. Maeder, C. J. Meyer, A. D. Zuberbühler, *Talanta* **1985**, *32*, 257–264; c) H. Gampp, M. Maeder, C. J. Meyer, A. D. Zuberbühler, *Talanta* **1985**, *32*, 1133–1139; d) H. Gampp, M. Maeder, C. J. Meyer, A. D. Zuberbühler, *Talanta* **1986**, *33*, 943–951.
- [22] P. F. Wang, L. Jullien, B. Valeur, J.-S. Filhol, J. Canceill, J.-M. Lehn, *New J. Chem.* **1996**, *20*, 895–907.
- [23] Left: movie displaying the temporal evolution of the epifluorescence image of the PDMS microfluidic device initially containing $(80 \pm 5) \mu\text{M}$ $\text{cS}_1^{\text{OMe}}\text{D}$ upon photoactivation at $\lambda_{\text{exc}} = (360 \pm 20) \text{ nm}$ with $2.5 \times 10^{-3} \text{ Ein s}^{-1} \text{ m}^{-2}$ light intensity and imaging at $\lambda_{\text{em}} = (675 \pm 45) \text{ nm}$. Right: temporal evolution of the fluorescence emission from six neighboring $\text{cS}_1^{\text{OMe}}\text{D}$ -containing wells (a vertical offset was introduced to facilitate reading). Markers: experimental data; red solid lines: fits with Equation (46) yielding $\langle k_1 \rangle = (0.116 \pm 0.003) \text{ s}^{-1}$ and $\langle k_2 \rangle = (1.11 \pm 0.07) \text{ s}^{-1}$. Solvent: $\text{CH}_3\text{CN}/0.1 \text{ M Britton-Robinson pH } 8 \text{ buffer } 1:1 \text{ (v/v)}$; $T = 293 \text{ K}$.

Received: April 6, 2013
Published online: July 16, 2013